Accuracy Analysis of Radiometric Calibration In-Orbit for SuperView Neo-2 SAR Satellite

Huijuan Li, Heng Zhang, *Member, IEEE*, Qi Chen, Yongpeng Gao, *Member, IEEE*, Xiaoyu Shi, and Lifeng Zhang

***Abstract*—The radiometric calibration technique of spaceborne synthetic aperture radar (SAR) aims to establish a constant relationship between the SAR target pulse response energy and the actual radar cross-section (RCS) of the ground. It is an essential technology for achieving quantitative observations of the Earth using radar. In this article, the process of in-orbit radiometric calibration campaign for the SuperView Neo-2 SAR satellite is introduced, which is the distributed X-band SAR satellite in the new generation of Chinese SiWei commercial remote sensing satellite system. More specifically, the initial step involves deriving the total transfer function of the SAR system using the radar equation and establishing a stable calibration constant model for the SAR system. Further, by using the obtained calibration constant to invert the RCS value of the corner reflectors in the Otog Banner calibration field, while validating and analyzing the absolute radiometric accuracy. Considering that the elevation antenna pattern (EAP) predominantly affects the consistency of image radiometric correction, the method of extracting EAP and beam center bias angle from the rainforest is presented. Finally, the quality validation of impulse response function is performed over the California calibration field, which can effectively guarantee the quality of SuperView Neo-2 SAR satellite products.**

***Index Terms*—Impulse response function, radiometric calibration, SuperView Neo-2 SAR satellite, synthetic aperture radar (SAR).**

I. Introduction

THE SuperView Neo-2 synthetic aperture radar (SVN2-SAR) satellite belongs to China SiWei Surveying and Mapping Technology Company, Ltd. of the China Aerospace Science and Technology Corporation. It features X-band commercial SAR satellite with high-resolution imaging capability. The sliding spotlight (SS) provides a resolution better than 1 m, while the Stripmap (SM) provides 2-m resolution. The SVN2-SAR satellite has the capability to acquire radar interferometric data under all weather conditions throughout the day [1]. It enables the rapid survey and production of global, high-resolution digital surface model or digital elevation model and digital orthophoto map at a scale of 1:25000. Additionally, SVN2-SAR possess the advanced capability to perform differential interferometric missions employing the "double satellite formation flying" mode, which effectively supports the construction of global geographic information framework, and provides commercial remote sensing data services for geological and geomorphic exploration, disaster prevention and reduction, and mineral resource monitoring or other industries.

The extensive usage of the SVN2-SAR satellite across various industries and fields has posed challenges for traditional qualitative remote sensing to meet its high-precision imaging requirements. Furthermore, the signal processing of the SAR system introduces numerous gain errors, resulting in SAR images that fail to accurately depict the echo characteristics of real ground objects. Consequently, this directly hinders the quantification application of SAR high-resolution images. Hence, it becomes essential to address various errors such as in-orbit errors, propagation errors, and external calibration errors through SAR satellite calibration processing. This approach enables quantitative observation of the ground and enhances the stability of satellite imaging. Quantitative remote sensing technology has progressively emerged as a vital method for optimizing the performance of spaceborne SAR systems.

The radiometric calibration technology for spaceborne SAR is a crucial step in achieving quantitative remote sensing [2], [3]. Radiometric calibration involves both internal and external calibration. Internal calibration focuses on measuring the amplitude and phase characteristics of the antenna TR channel and the system reference function to calibrate radar system performance. External calibration, on the other hand, utilizes echo signals from corner reflectors (CRs) or active calibrators during field experiments [4]. In particular, the external calibration campaign for spaceborne SAR enables precise retrieval of radar scattering cross-section from SAR images [5], [6], [7], thus laying the foundation for subsequent quantitative applications of radar products. In the development stage of China's commercial remote sensing satellites, there is a scarcity of literature specifically addressing radiometric calibration based on these commercial SAR satellites. At present, some publicly available literature relies on foreign SAR satellites for research purposes. For instance, Tao et al. [8], in their 2015 publication, validated the modeling methodology of spaceborne SAR radiometric accuracy using TerraSAR-X satellite of German. Additionally, some studies employ simulation data for radiometric calibration research. For example, in 2000, Peng et al. [9] verified the

Manuscript received 29 July 2023; revised 25 September 2023 and 3 November 2023; accepted 30 November 2023. Date of publication 13 December 2023; date of current version 3 January 2024. This work was supported by Commercial Remote Sensing Satellites System Project of China Aerospace Science and Technology Corporation. *(Corresponding author: Heng Zhang.)*

The authors are with the China Siwei Surveying and Mapping Technology Company, Ltd., Beijing 100190, China (e-mail: mearing@foxmail.com; zhangheng01@radi.ac.cn; chenq_cn@163.com; godneos971027@gmail.com; 2754087017@qq.com; 2217197640@qq.com).

Digital Object Identifier 10.1109/JSTARS.2023.3342437

imaging gain error in radiometric calibration through the utilization of simulation data. Consequently, conducting research and analyzing the accuracy of in-orbit radiometric calibration technology specifically tailored to China's commercial SVN2-SAR satellite holds immense significance in achieving precise quantification of high radiometric precision radar products.

After the SVN2-SAR satellite is launched, the imaging mission planning system forecasts the scheduled path for the calibration field in advance. The ground system's field test team subsequently installs CRs within the designated calibration field. This enables the ground processing system to carry out a comprehensive array of tests, including radiation calibration, to evaluate the integration performance between the satellite and the Earth. This article focuses on the radiometric calibration campaign and quality validation of SVN2-SAR. First, the total transfer function of the satellite system is derived by applying the radar equation. This derivation leads to the establishment of a calibration constant model for the stable SAR system. After obtaining the calibration constants of the satellite, the measured radar cross-section (RCS) of CRs is further inverted using the known RCS nominal value. The absolute radiation accuracy is then analyzed by utilizing the measured RCS. Furthermore, it is essential to note that precise measurement of the satellite antenna pattern and beam pointing has a decisive impact on the radiometric accuracy of SAR images [10]. Since the SVN2-SAR satellite is characterized by its lightweight, small size, and agility, its antenna system adopts a feed array configuration along with an umbrella-shaped parabolic reflector. The antenna system such as SVN2-SAR cannot achieve high accuracy beam orientation angle determination by transmitting differential beams like active phased array antenna satellites (such as Gaofen-3 series SAR satellites). Therefore, this article proposes a method to measure the EAP and beam bias of the SVN2-SAR reflector antenna system by utilizing measured natural surface data. Finally, the article conducted assessment of the IRF quality: spatial resolution, peak sidelobe ratio (PSLR), and integrated sidelobe ratio (ISLR) of CRs from SM in the California calibration field. This allowed for the quantitative evaluation of the imaging quality of the SVN2-SAR satellite, providing a solid foundation for its subsequent application in different fields such as land surveying, mapping, and marine environmental protection.

II. Precursors

Spaceborne SAR radiometric calibration technology establishes a consistent relationship between radar image scattering characteristics and observed scenes through the total transfer function of the SAR system. In a stable SAR system, this transfer function is typically represented by a fixed constant known as the satellite calibration constant [11], [12], [13]. The satellite ground processing system can achieve absolute radiometric correction of SAR images by measuring calibration constants through field campaigns. However, several error sources within the SAR system, such as antenna pattern measurement errors and beam pointing errors, can impact the accuracy of SAR radiometric calibration [14]. Therefore, measuring satellite antenna patterns and beam pointing is crucial to improve the accuracy of satellite radiometric calibration. Moreover, the calibration campaign includes SAR image quality validation to evaluate the imaging capability of the SVN2-SAR satellite.

A. Construction of Calibration Constant Model

Spaceborne SAR satellites achieve high-resolution imaging by transmitting linear frequency modulation signals and continuously receiving ground-reflected echo signals [15], [16], [17]. During the field calibration campaign, after the satellite passes over the area where CRs are placed on the ground, the average power P_r of the ground CRs echo signal received by the SAR payload can be expressed as follows [18], [19], [20]:

$$P_r = \frac{P_t G^2(\varphi_r, \varphi_a) G_{sp} \lambda^2 \sigma}{(4\pi)^3 R^4} + P_n \tag{1}$$

where P_t represents the power of the satellite transmission signal. Taking SVN2-SAR monostatic transceiver imaging as an example, when the antenna transmit and receive gains are equal, then $G^2(\varphi_r, \varphi_a)$ corresponds to the telemetry and command (T&C) antenna pattern. φ_r and φ_a denote the elevation and azimuth angles of the satellite, respectively. G_{sp} indicates the system processing gain. λ represents the wavelength at which the linear frequency modulation signal is transmitted. σ signifies the RCS of the observed scene/target. R represents the slant range distance between the radar and the target. Finally, P_n represents the thermal noise power of the SAR system. It can be observed from (1) that achieving high-precision satellite calibration requires accurate measurement of the gains of the SAR system, as well as the equivalent values of slant range distance and RCS. In practical SAR systems, internal calibration technology is commonly employed to measure the relative changes in gain for accomplishing relative calibration [21], [22], [23]. This technology enables the comparison of current measurements with reference data to assess any variations in gain over time. By utilizing relative calibration techniques (different from relative radiometric correction), the SAR system can maintain its accuracy and reliability throughout its operation. In addition, the RCS value of the target must be measured using radiative external calibration technology. This is crucial for achieving accurate SAR radiometric calibration.

Based on the average power P_r of the received echo signal from the SAR payload, a linear relationship model is further developed, considering the transfer function H of the SAR system

$$P_r = H\sigma. \tag{2}$$

For a stable satellite payload system, the total transfer function H of the SAR system remains constant within a specific linear dynamic range. This constant, known as the absolute calibration constant K, needs to be determined through a radiative external calibration campaign. The calculation of the K value in the external field calibration campaign relies on the energy value of the impulse response derived from standard reference CRs extracted from SAR images. To avoid errors in response energy extraction caused by image focusing, the SVN2-SAR satellite calibration

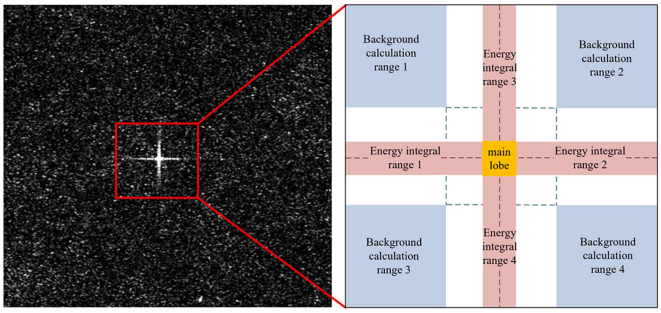

Fig. 1. Impulse response energy extraction of CR.

employs the integral method for extracting the response energy of the CRs [24], [25], [26]. The window structure of the CR energy integration area is illustrated in Fig. 1.

The left figure of Fig. 1 shows the imaging results of the CR of the calibration field SS mode of the SVN2-SAR satellite over the Otog Banner, where the nominal resolution of the SS mode is 1 m and the side length of the CR is 1.204 m. The right figure of Fig. 1 is a schematic diagram of the response energy calculation of the CR. The response energy value of the CR can be obtained by calculating the difference between the energy value of the range of the red cross part in the right figure of Fig. 1 and the range of the background 4 blocks, which is calculated as follows:

$$Q_{\mathrm{CR}} = \left(\sum_{i \in A}^{N_A} \mathrm{DN}_i^2 - \frac{N_A}{N_B} \sum_{i \in B}^{N_B} \mathrm{DN}_i^2 \right) \gamma_r \gamma_a \tag{3}$$

where A represents the range of energy integration from 1 to 4 in the right figure of Fig. 1, and B represents the range of background calculation from 1 to 4. N_A and N_B denote the total number of pixels within the energy integral range and the background range, respectively. DN_i represents the pixel digital number (DN). For satellite SLC products, DN_i is the amplitude value of a pixel: $\mathrm{DN}_i = \sqrt{I^2 + Q^2}$, where I and Q are the real and imaginary values, respectively. Thus DN_i^2 represents the pixel power value. γ_r and γ_a denote the pixel spacing in the range and azimuth, respectively. Thus, the relationship between the energy of the CR extracted from SAR images and the actual RCS of ground CR can be further established as follows:

$$Q_{\mathrm{CR}} = P_r \rho_r \rho_a = K \sin\theta \sigma_{\mathrm{CR}} \tag{4}$$

where ρ_r is the range resolution, ρ_a is the azimuth resolution, θ is the incidence angle, and σ_{CR} is the nominal RCS value of the CR deployed in the external field. In (4), it is evident that accurately extracting the response energy of the reference CR in SAR images is of vital importance for calculating the total transfer function (calibration constant) of a stable SAR system. The corresponding logarithmic power formula can be further derived as follows:

$$10\lg\left(Q_{\mathrm{CR}}\right) = 10\lg\left(K\right) + 10\lg\left(\sigma_{\mathrm{CR}}\right) + 10\lg\left(\sin\theta\right). \tag{5}$$

Moreover, to further enhance the radiative calibration accuracy of the field calibration campaign, the calibration constant is typically calculated by extracting the response energy values from multiple reference targets. The singular value is eliminated, and the average value is obtained. Consequently, the final calibration constant can be expressed as follows:

$$K = \frac{1}{L} \sum_{j=1}^{L} K_j \tag{6}$$

where L is the number of calibration devices deployed in the calibration field.

B. Derivation of EAP Through the Radar Equation

The satellite antenna pattern plays a crucial role in ensuring accurate radiation during satellite imaging and is a key factor in SAR radiation calibration [27], [28]. Prior to satellite launch, ground testing is conducted to establish the theoretical radiation pattern. However, it is important to note that the conditions in outer space cannot be fully replicated in the ground test environment. Factors such as rocket vibrations, temperature variations, and the presence of space debris during launch can potentially cause damage to the satellite antenna. Consequently, the actual antenna pattern may deviate from the theoretical pattern.

To address these challenges, in-orbit measurement of the satellite antenna pattern is essential. By conducting measurements in the actual operating environment of the satellite, the radiation performance of satellite imaging can be effectively guaranteed. Conducting in-orbit measurements enables the acquisition of more precise antenna radiation patterns. Through appropriate compensation and calibration of antenna patterns, the optimal radiometric accuracy of satellite imagery can be guaranteed. Therefore, the in-orbit measurement of the satellite antenna pattern significantly contributes to improving the overall quality and reliability of satellite imaging.

The antenna pattern of a satellite is typically categorized into two components: the elevation antenna pattern (EAP) and the azimuth antenna pattern. The azimuth antenna pattern measurement depends on the ground receiver, and it generally aligns well with the reference ground test pattern. It is the EAP that significantly influences the radiation accuracy of SAR products. In order to achieve accurate measurements, the natural features of the Amazon rainforest (RF) are commonly utilized in conducting in-orbit measurements of the EAP.

The Amazon RF region, spanning across several countries in South America, is not only the world's largest tropical RF but also a unique and valuable resource for satellite calibration [29], [30], [31]. The expansive and uniformly backscattering nature of the Amazon RF makes it an ideal target for measuring and calibrating satellite imaging antenna radiation patterns. Moore et al. [32], pioneers in their field, recognized the immense potential of the Amazon RF for in-orbit measurement of antenna patterns. Consequently, the natural elements of the RF can be employed as the external calibration campaign field of the SAR antenna pattern. The radar equation for distributed targets can be expressed as

$$P_{r\_\mathrm{RF}} = \frac{P_t G^2\left(\varphi_r, \varphi_a\right) G_{sp} \lambda^3 \rho_r \tau_p f_s f_{\mathrm{PRF}}}{2(4\pi)^3 R^3 V \sin\theta} \sigma \tag{7}$$

where τ_p is the pulse width of the linear frequency modulation signal, f_s is the range sample frequency, f_{PRF} is the pulse

repetition frequency of the satellite transmitted signal, and V is the satellite flight speed. The radar equation of uniformly distributed targets can be simplified after relative correction on the satellite

$$P_{r\_\mathrm{RF}} = \frac{G^2(\varphi_r, \varphi_a)}{R^3 \sin\theta} K\sigma. \tag{8}$$

By solving the gain value corresponding to each range gate, the EAP of the satellite can be extracted, and its mathematical model may be created as

$$G^2(\varphi_r, \varphi_a) = P_{r\_\mathrm{RF}} \bullet \frac{R^3 \sin\theta}{K\sigma}. \tag{9}$$

Since the corresponding gain of SAR images without theoretical pattern radiation correction is different for different range gates, the elevation look angle corresponding to the maximum gain (normalized to 0dB) is the actual elevation look angle of the radar antenna beam center. By combining with mission planning, the working angle of the radar antenna beam can be obtained, and the beam bias angle of the reflector antenna system satellite can be measured.

C. SLC Products Quality Metrics: IRF

By employing a subjective and qualitative approach, it becomes straightforward to identify issues such as defocusing and blurring of the SLC products. However, in order to monitor the quality of SAR images more accurately, SAR images still need to be quantitatively evaluated. The SVN2-SAR satellite evaluates image quality by computing the Impulse Response Function (IRF), which is based on ground-deployed CRs. The IRF primarily encompasses the measurement of image resolution and sidelobe levels. By acquiring measured values, it is possible to validate whether the satellite image quality and sidelobe levels meet the intended design standards.

1) Spatial Resolution: The spatial resolution of the SAR image is divided into range resolution and azimuth resolution. In general, the slant range resolution is defined as the main lobe width of the CR's extension function at the half-power point (3 dB) in the range direction. In the process of IRF quality validation, the first calculation is to get the slant range resolution ρ_{slant}. Then, the slant range resolution is converted to ground range resolution by applying the satellite-ground geometry relationship. The transformation between slant range resolution and ground range resolution is as follows:

$$\rho_{\mathrm{ground}} = \frac{\rho_{\mathrm{slant}}}{\sin\theta_i} = \frac{c}{2f_s \cdot m \cdot \sin\theta_i} \cdot N_r \tag{10}$$

where c is the speed of light, and f_s is the range sampling frequency, and m is a multiple of the range to the interpolation. Similarly, the azimuth resolution ρ_a is defined as the main lobe width of the CR's extension function at the half-power point (3 dB) in the azimuth direction

$$\rho_a = \frac{v_g}{f_{\mathrm{PRF}} \cdot n} \cdot N_a \tag{11}$$

where v_g is the velocity of the zero-doppler plane, and n is a multiple of the azimuth to the interpolation.

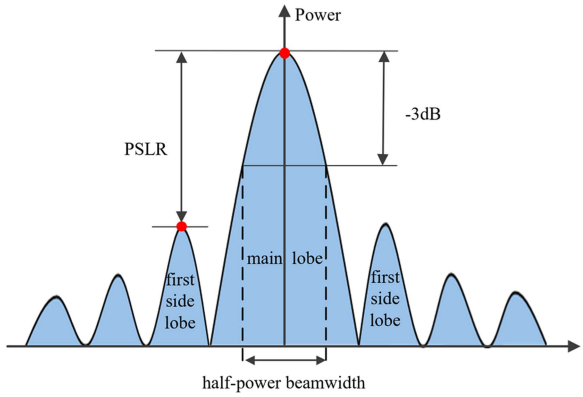

Fig. 2. Schematic diagram of SAR point target PSLR calculation.

2) Peak Sidelobe Ratio/Integrated Sidelobe Ratio: The PSLR refers to the ratio between the peak power of the first sidelobe and the peak power of the main lobe in the point target, which quantitatively describes the detection performance of the SAR load to the weak signal of the ground [33], and the specific calculation formula can express as

$$\mathrm{PSLR} = 10\lg\frac{P_s}{P_m} \tag{12}$$

where P_s is the peak of the first side. P_m is the main value peak. The calculation of the PSLR is shown in Fig. 2.

The integral side lobe represents the ratio of the main lobe energy to the side lobe energy in the target impulse response profile [34]. First, the main lobe energy is calculated at the main lobe peak, and then the side lobe energy is calculated outside the main lobe window. The specific calculation formula can be expressed as

$$\mathrm{ISLR} = 10\lg\frac{\int_{-\infty}^{a}|h(r)|^2dr + \int_{b}^{\infty}|h(r)|^2dr}{\int_{a}^{b}|h(r)|^2dr} = 10\lg\frac{E_s}{E_m} \tag{13}$$

where the integral limit (a, b) is the main value and the remaining range is the side lobe area. $h(r)$ indicates the curve function of the point target in the image domain along the range or azimuth. E_s is the total energy of the side lobe, and E_m is the main lobe energy.

III. Processing Flowchart

To summarize the processing procedure of the radiometric calibration processing and IRF quality validation of SAR image quality, Fig. 3 is given to demonstrate the flowchart. The field radiation calibration campaign is mainly aimed at point targets and distribution targets. However, the point targets and distribution targets are interrelated and complementary, and only precise calibration can be used to ensure that the satellite provides radiation-quantifying products.

Errors in relative radiometric calibration during the SAR imaging process directly lead to inaccuracies in the absolute radiometric calibration constants, thereby impacting the precision of absolute radiometric measurements. Furthermore, the

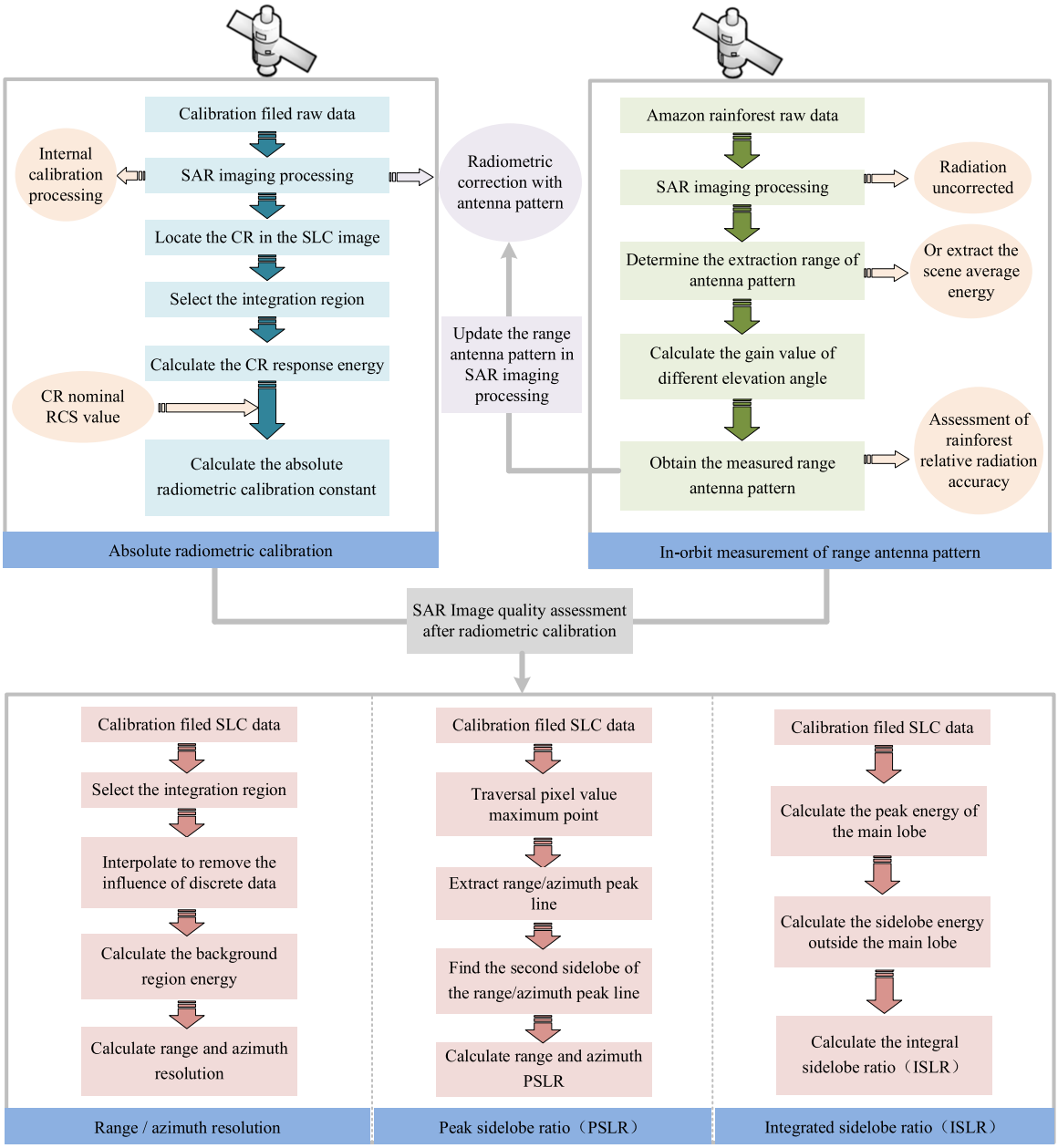

Fig. 3. Processing flowchart of the SVN2-SAR radiometric calibration and IRF quality validation.

accuracy of relative radiometric calibration depends on the precise acquisition of the EAP. Therefore, performing regular in-orbit monitoring of the EAP normalization can effectively ensure the radiation quality of SVN2-SAR satellite products.

In addition, conducting a quality assessment of SAR images using the metric IRF is necessary. Prior to satellite launch, a series of imaging performance indicators are established, such as satellite theoretical resolution, signal sidelobe level. And the IRF serves as an effective tool to validate the actual imaging capabilities of satellites. The imaging capability of satellites has a significant impact on the subsequent applications of remote sensing products, particularly regarding the quality of SAR images and target detection. Excellent imaging capability provides high spatial resolution, and low sidelobe levels, resulting in clear and detailed images. This has a positive impact on various applications, including environmental monitoring, resource management, and military intelligence. Through high-quality satellite imaging, surface targets can be observed and identified more accurately, providing a reliable foundation for subsequent data analysis and decision-making.

IV. Calibration and Validation

A. *Preparation of Radiometric Calibration Campaign*

The SVN2-SAR satellite was launched on July 16, 2022, from the Taiyuan Satellite Launch Center. The Long March-2C carrier rocket successfully placed the SVN2-SAR satellite into its designated orbit. Subsequently, the ground processing system

conducted the initial phase of on-orbit testing for satellite-Earth integration, primarily focusing on monostatic imaging. To fulfill the demands of satellite in-orbit testing, it is imperative to accurately select the calibration area through scientific means. The following are the four standards and specifications that must be met for the selection of a satellite in-orbit calibration filed.

1) The calibration area should be flat and ideally situated in an open space. The open space helps to eliminate any layover or shadow on the SAR image, thereby highlighting the imaging points of the CRs for easier and more accurate positioning.
2) The calibration area should consist of a homogeneous land cover type in order to prevent the multipath effect on the imaging points of the CRs caused by the surrounding objects.
3) The east–west extent of the calibration area should be sufficient to encompass the two standard SAR image.
4) The north–south extent of the calibration area should be sufficient to encompass the one standard SAR image.

By conducting multiple field surveys and coordination, the optimal locations for external calibration campaigns can be determined based on site selection standard. The next step is to lay out the CRs. The following are the standards that should be followed for the deployment campaign of CRs.

1) The CRs should be placed in an area with minimal background reflection to facilitate its effective extraction from the SAR image.
2) To optimize performance, it is recommended to position the CRs away from objects that may cause multipath effects or exhibit strong scattering characteristics.
3) When installing the CRs, ensure that the CRs base does not receive radar waves.
4) The edge below the CRs should be aligned parallel to the direction of the satellite track.
5) The normal of the CRs should be aligned with the incident direction of the radar wave.

In conclusion, according to the standards for site selection and CRs deployment, the location for the external field calibration campaign of the SVN2-SAR satellite is conducted in Otog Banner (Inner Mongolia, China).

The distribution of the Otog Banner calibration field on Google Earth is depicted in Fig. 4.

The Otog Banner calibration field in Fig. 4 is equipped with nine trihedral CRs, which are arranged in line A and labeled as A01–A09. This arrangement allows for precise calibration measurements to be taken within the designated area. The CR device has a pitch adjustment accuracy of better than 0.15°, allowing for precise angle adjustments during reflection. Its side length measures at 1.204 m, providing information on its nominal RCS calculation for data processing purposes. Calculating the RCS of CR in SAR Image using its side length and satellite wavelength: $\sigma_{\text{ref}} = 4\pi a^2/3\lambda^2$, where σ_{ref} is the theoretical RCS value, a is the side length of CR, λ is the wavelength of the electromagnetic wave emitted by the SVN2-SAR satellite. The theoretical RCS value of the CR in X-band SVN2-SAR satellite image can be calculated as 39.5547 dB.

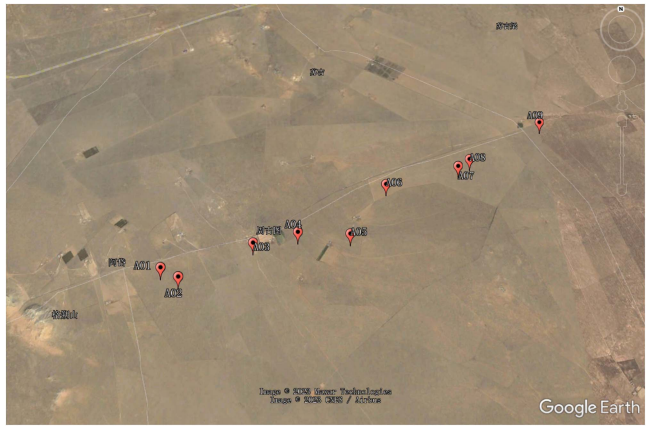

Fig. 4. Location of CRs in the Otog Banner calibration site.

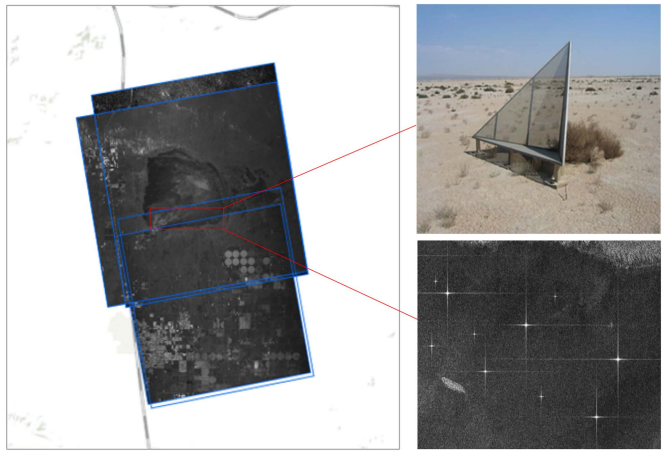

Fig. 5. California calibration field CRs distribution.

Due to the diverse terrain features and scattering characteristics present in each calibration site, conducting calibration using multiple sites provides a comprehensive understanding of the response and performance of SAR systems. Consequently, for the validation of IRF quality, California calibration field were utilized to acquire images of CRs to enhance data quality and ensure reliable validation results.

The distribution of California calibration field CRs is shown in Fig. 5.

The left image in Fig. 5 depicts the calibration field situated on the dry lakebed of Rosamond, in California. This image was captured using the SM mode by the SVN2-SAR satellite, which provides a detailed overview of the calibration site. The calibration field covers about 1 km × 10 km, and the latitude and longitude of the calibration field are 118.099°W–118.027°W, 34.795°N–34.806°N. The Rosamond calibration site is equipped with high-precision trihedral CRs of varying sizes. The right image in Fig. 5 shows a CR with a side length of 4.8 m in the upper right corner, and part of the CRs is displayed on the SAR image.

Once the field calibration site location is determined and the CRs are deployed, the prediction of the satellite imaging area is

TABLE I
PARAMETERS FOR SVN2-SAR SATELLITE

Parameters	Value
Frequency band	X-band
Center frequency	9.6 GHz
Antenna system	Parabolic reflector
Imaging mode	SS/SM
Range of incidence angles	20°– 50°
Satellite Altitude	496.3 km
Orbital period	17day
Absolute radiation accuracy	≤1.5 dB
Relative radiation accuracy	≤1.0 dB
PSLR	≤–22 dB
ISLR	≤–14 dB

carried out. The prediction of the imaging area and the inference of coverage area require the utilization of the orbital elements transmitted by the T&C receiving station, along with consideration of the satellite's orbital ascent and descending mode and its side-swing capability. Among them, the six elements of a satellite orbit include semi-major axis, eccentricity, orbital inclination, argument of perigee, right ascension of ascending node, and true anomaly. According to these elements, the image and coverage area of the satellite in transit can be approximated. Accurately predicting the imaging and coverage regions is crucial for field calibrators to select the optimal calibration site and formulate a precise calibration scheme.

After deducing the satellite imaging and coverage areas, the final step in calibration preparation is to develop a comprehensive calibration campaign plan for the field calibration personnel. This involves coordinating with satellite planners to ensure that the emergency task arrangements of the satellite are not compromised.

B. Absolute Radiation Calibration and Accuracy Validation

The main parameters of the SVN2-SAR SAR satellite are shown in Table I.

The SM data of the SVN2-SAR satellite, with a nominal resolution of 2 m, were utilized as an illustrative example for conducting absolute radiometric calibration campaign. First, the beam coverage is analyzed in the Otog Banner calibration field based on the imaging mode and precise orbit information of the satellite. The azimuth and elevation angles of each CR are then predicted and adjusted accordingly. When the satellite passes over, it acquires the original Zero-level echo data of the calibration field and processes it for imaging. Some outliers need to be eliminated, which may be unavailable due to unexpected circumstances (such as the CRs being destroyed by cattle in the pasture) or the CRs are not adjusted because it conflicts with another imaging plan. After removing outliers, five CRs (A01, A02, A04, A06, A07) with known RCS values are effective devices in the SLC product. Two CRs (A01 and A02) were selected for calculating the calibration constants, and Fig. 6 illustrates the distribution of CRs in the SAR image. The SM mode imaging of the SVN2-SAR satellite in Otog Banner calibration field is showcased, along with the magnified image of the point target and the physical image of the actual CR. Fig. 6 clearly illustrates that there is an optimal spacing maintained between the CRs to prevent energy interference among the imaging points of different reflectors. This approach plays a crucial role in accurately extracting the energy values of the CRs.

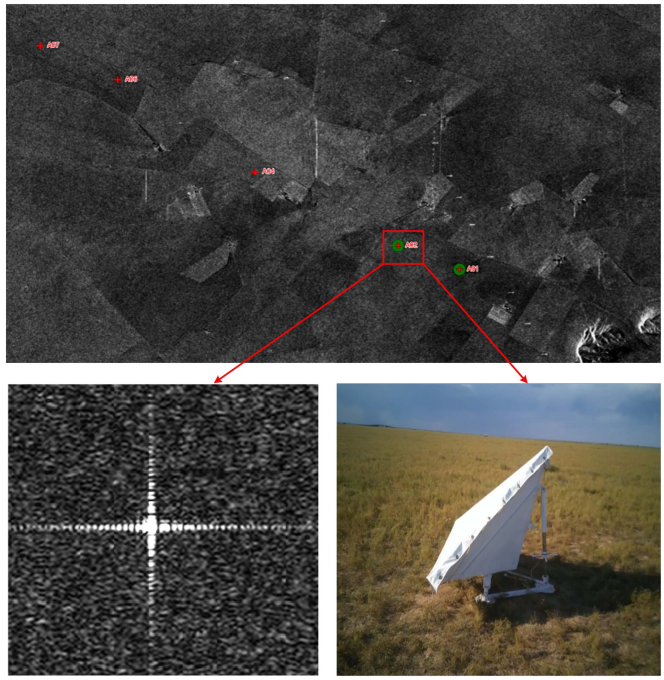

Fig. 6. CRs for absolute radiation calibration constant measurement.

TABLE II
RESULTS OF ABSOLUTE RADIATION CALIBRATION CONSTANT

Number	CR	RCS/dB	Energy value/dB	Calibration constant/dB
1	A01	39.5547	30.08	–9.4747
2	A02	39.5547	29.38	–10.1747
Mean value			29.73	–9.8247

TABLE III
RESULTS OF ABSOLUTE RADIATION ACCURACY VALIDATION

Number	CR	RCS/dB	Inversion RCS /dB	Measuring error /dB
1	A04	39.5547	38.4418	1.1129
2	A06	39.5547	38.9523	0.6024
3	A07	39.5547	38.0635	1.4912
Absolute radiation accuracy /dB				≤1.5dB

Then, according to the calibration constant model constructed in Section II-A, the calibration constants of SVN2-SAR satellite SM mode are calculated and presented in Table II.

The RCS values of the remaining three CRs (A04, A06, and A07) are inverted using the calibration constant −9.8247, and their absolute radiation accuracy is subsequently validated. The results of accuracy validation are presented in Table III.

The absolute radiation accuracy of the SM mode is observed to meet the radiation index specified in Table I (with a deviation of less than 1.5 dB in one scene). Therefore, it can be concluded that the calibration constant value provided in Table II is reliable.

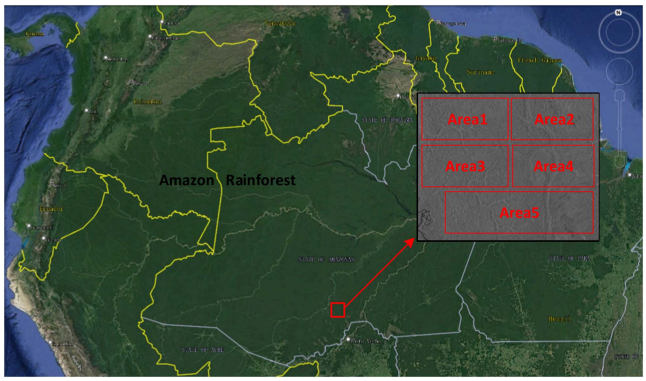

Fig. 7. Location of SLC products in the Amazon RF.

TABLE IV
RESULTS OF RF GAMMA VALUE

Number	Range samples	Azimuth samples	σ^0_{db} /dB	γ^0_{db} /dB
Area 1	11029	5514	−7.0358	−6.1951
Area 2	11365	5333	−7.0746	−6.2339
Area 3	10770	5307	−7.0826	−6.2419
Area 4	11210	5385	−7.0989	−6.2582
Area 5	20504	6394	−7.1400	−6.2993
Mean value /dB			−7.0864	−6.2457

To further validate the accuracy of calibration constant from additional perspectives, cross-radiometric calibration was employed to retrieve the backscattering coefficient of the RF using natural features. The location of the Amazon RF is shown in Fig. 7.

By imaging the flat areas of the Amazon RF, we have successfully acquired SM mode SAR Level-1 SLC products. To obtain a more accurate inversion of gamma values for RF s, the data were partitioned into five blocks and subjected to distributed calculations prior to averaging. In addition, the relationship between σ^0 and γ^0 is $\sigma^0/\cos(\alpha) = \gamma^0$, where α is the incidence angle. First, calculate the energy value of each distributed target block and subtract the obtained calibration constant from the energy value. Then, utilize the aforementioned relationship to perform the conversion and the γ^0 value of the RF target can be inversely inferred. Generally, theγ^0_{db} value of X-band SAR is around -6.5 dB [35]. The results of RF γ^0_{db} value as shown in Table IV, validating that the calibration constant is reliable and accurate.

C. EAP Measurement in Orbit

The accuracy of satellite radiation correction is significantly influenced by the EAP. The SVN2-SAR satellite's EAP is measured in orbit using the natural calibration field of the Amazon RF. First, telemetry parameters are transmitted and mission remote control instructions are uploaded through the satellite measurement and control system. Then, based on orbital prediction information, the zero Doppler slant distance between the satellite and center point of the scene in the first imaging region is calculated. The working angle of the radar beam pointing to the center of the scene is calculated according to the orbit

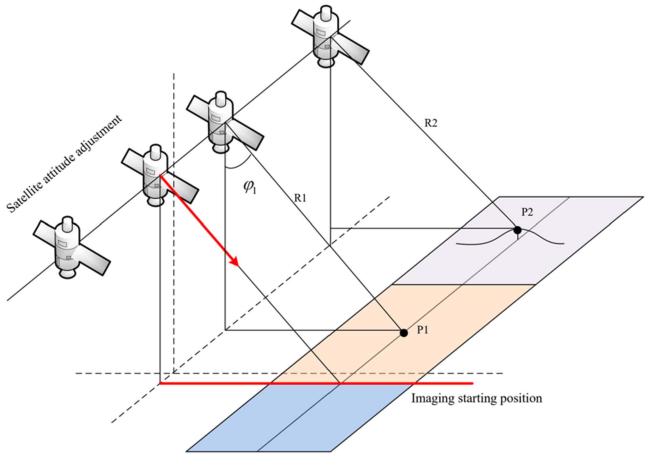

Fig. 8. Illustration of satellite SM imaging.

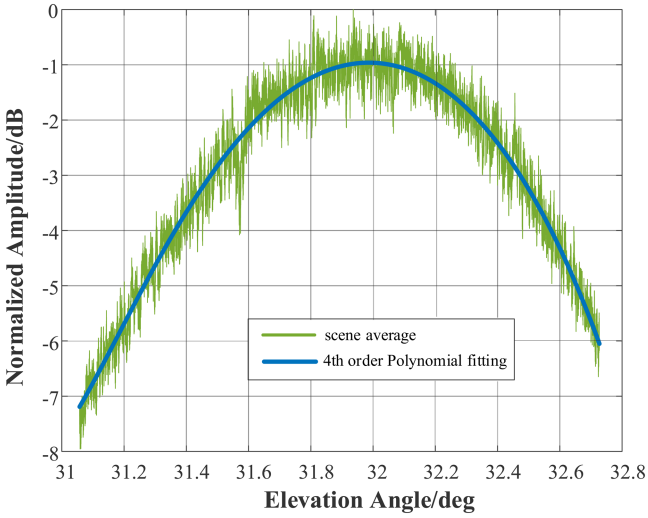

Fig. 9. EAP extracted from RF.

altitude and other information. Prior to the imaging starting position, adjustments are made to the attitude of satellite so that the working angle of the radar beam center aligns with φ_1 while maintaining the same for the imaging block. The process is depicted in Fig. 8. In Fig. 8, P1 represents the scene center of the first imaging area, and R1 represents the slant range corresponding to the scene center of the first imaging area. φ_1 is the working angle of the radar antenna beam center.

The satellite receiving system is utilized to acquire the raw echo complex data of the Amazon tropical RF. Subsequently, this raw echo complex data undergoes imaging processing in order to generate an SAR image without radiation correction (single-look complex image). Then the EAP was calculated using the technical route constructed in Section II-B. The gain was determined by selecting the scene average of azimuth. To fit the measured range antenna, a polynomial fitting model was utilized. The EAP extracted from the RF SM mode of the SVN2-SAR satellite is presented in Fig. 9, along with the EAP that has been fitted using a fourth-order polynomial.

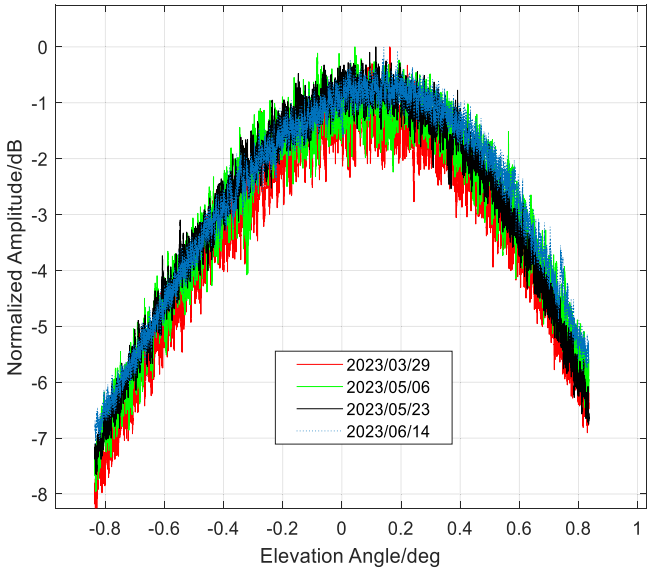

Fig. 10. EAP of different time series.

After extracting the EAP based on evenly distributed targets in an RF, it is possible to obtain the actual angle of the radar antenna beam center corresponding to the maximum gain of the pattern. By combining this information with the working angle of the radar antenna beam center during mission planning, it is possible to calculate the satellite beam center bias angle

$$\varphi_{\text{beam bias}} = \varphi_{\text{work angle}} - \varphi_{\text{RF\_elevation angle}}$$

where $\varphi_{\text{beam bias}}$ is the radar antenna beam center bias. By compensating this value in the SAR ground imaging process, the radiation correction accuracy of radar images can be effectively achieved. $\varphi_{\text{work angle}}$ is the working angle of the radar antenna beam center. For SM, each image block has the same looking angle, so $\varphi_{\text{work angle}} = \varphi_1$. Due to the unknown factors in the operation of the satellite with the parabolic reflector antenna system, there will be a deviation between the beam center working angle and the final imaging angle. $\varphi_{\text{RF\_elecation angle}}$ represents the true elevation angle extracted from the measured RF data, which is the angle corresponding to the maximum gain of EAP measured in orbit.

In addition, dynamic monitoring of satellite imaging can be achieved by accumulating sequential data from satellite RF and regularly extracting EAP of RF data from different dates. This process allows for accurate tracking and analysis of changes in satellite beam pointing, which can have important implications for satellite operation and imaging. Fig. 10 shows the EAP of a different date.

In order to verify the radiation correction effect of the measured EAP, the relative radiation accuracy of the RF corrected by the extracted EAP was measured. As shown in Table V.

Table V illustrates the relative radiation accuracy of four sets of RF data at different time intervals. Each RF image was equally partitioned into nine regions, and response energy was calculated for each region to determine the relative radiation accuracy. The SVN2-SAR satellite demonstrated strong radiation correction stability across various time periods, resulting in excellent image radiation performance. This time-series data enable effective monitoring of satellite radiation performance.

TABLE V
RESULTS OF RELATIVE RADIATION ACCURACY VALIDATION

RF	Number	Incidence/deg	Energy/dB	Relative radiation accuracy/dB
2023/03/29	Area 1	34.15032	−17.8563	0.732654
	Area 2	34.77132	−17.4828	
	Area 3	35.37517	−17.6635	
	Area 4	34.15032	−17.2313	
	Area 5	34.77132	−17.3639	
	Area 6	35.37517	−17.7151	
	Area 7	34.15032	−17.2643	
	Area 8	34.77132	−17.2118	
	Area 9	35.37517	−17.8298	
2023/05/06	Area 1	34.11036	−17.9004	0.729512
	Area 2	34.72838	−17.6334	
	Area 3	35.32937	−17.3759	
	Area 4	34.11036	−17.8172	
	Area 5	34.72838	−17.6797	
	Area 6	35.32937	−17.0879	
	Area 7	34.11036	−17.7099	
	Area 8	34.72838	−17.8656	
	Area 9	35.32937	−17.6724	
2023/05/23	Area 1	32.96763	−16.2890	0.664007
	Area 2	33.58302	−16.0127	
	Area 3	34.18142	−16.5750	
	Area 4	32.96763	−16.2854	
	Area 5	33.58302	−16.0862	
	Area 6	34.18142	−16.6388	
	Area 7	32.96763	−16.1922	
	Area 8	33.58302	−16.2635	
	Area 9	34.18142	−16.6436	
2023/06/14	Area 1	34.11789	−17.7074	0.815467
	Area 2	34.73778	−17.2891	
	Area 3	35.34055	−17.9436	
	Area 4	34.11789	−17.6710	
	Area 5	34.73778	−17.4675	
	Area 6	35.34055	−17.2084	
	Area 7	34.11789	−17.8005	
	Area 8	34.73778	−17.6886	
	Area 9	35.34055	−17.2794	

V. CONCLUSION

The SuperView Neo-2 X-band SAR in China SiWei Surveying and Mapping Technology Company, Ltd., commercial remote sensing system is utilized for radiometric calibration and IRF validation in this study. The RCS value of the CRs is retrieved from the calibration constant measured in the Otog Banner field campaign, ensuring the absolute radiometric calibration accuracy of the satellite. Additionally, RF is employed to validate the calibration constants, effectively guaranteeing accurate radiometric calibration. Furthermore, measurement methods are provided for EAP and beam bias angle which impact radiation accuracy. Sequential RF target data are used to extract the normal EAP, ensuring the long-term radiation performance of the satellite. Finally, the IRF quality validation of the SVN2-SAR image from the California calibration field enables quantitative monitoring of satellite imaging performance and ensures the

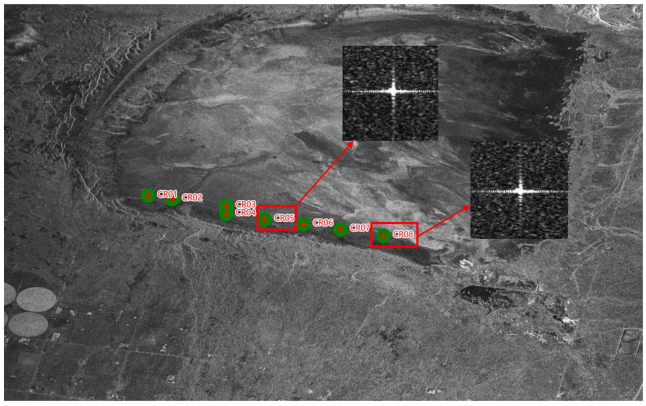

Fig. 11. California calibration field imaging by SVN2-SAR SM.

TABLE VI
RESULTS OF IRF QUALITY VALIDATION

Number	Azimuth/Range resolution/m	Azimuth/Range PSLR/dB	Azimuth/Range ISLR/dB
CR01	1.8099/1.9382	–30.0738/–22.9776	–23.9162/–22.3835
CR02	1.8013/1.9161	–30.9224/–22.7511	–25.0056/–22.6404
CR03	1.8700/1.9540	–30.3718/–23.9137	–24.0285/–21.3203
CR04	1.7626/1.9089	–31.3509/–22.3016	–24.8955/–22.4726
CR05	1.8056/1.9540	–29.8610/–23.2927	–24.1419/–19.8592
CR06	1.7970/1.9408	–31.4358/–23.5594	–23.9559/–19.5818
CR07	1.7626/1.9331	–31.3299/–24.1806	–24.3775/–19.4379
CR08	1.7411/1.9405	–30.5691/–23.3958	–23.9972/–20.0628
Max	1.8700/1.9540	–29.8610/–22.3016	–23.9162/–19.4379

high-quality product supply capability of the SVN2-SAR satellite.

APPENDIX

In accordance with the technical schemes in Section II-C, the SVN2-SAR impulse response function is validated in terms of

1) Ground range resolution;
2) Azimuth resolution;
3) Peak side lobe ratio;.
4) Integral side lobe ratio

The IRF of the SVN2-SAR satellite was validated by utilizing the California CRs, enabling the assessment of image quality. The SLC product of the California field is displayed in Fig. 11.

The CRs (CR01–CR08) in Fig. 11 underwent IRF quality validation, and the evaluation results are presented in Table VI.

Table VI demonstrates that the California calibration field CRs meet both peak side lobe ratio and integral side lobe ratio requirements, while also maintaining spatial resolution within the nominal 2 m for SM. To further evaluate point target quality, interpolation was performed using two CRs (CR05,CR08) and results are presented in Fig. 12.

After performing linear interpolation on the CR05 and CR08, the corresponding azimuth and range were extracted and are depicted in Fig. 13.

The main lobe of the point targets, as imaged by the SVN2-SAR satellite, exhibits clarity and a distinct target focus, effectively validating the imaging capabilities of the SVN2-SAR satellite.

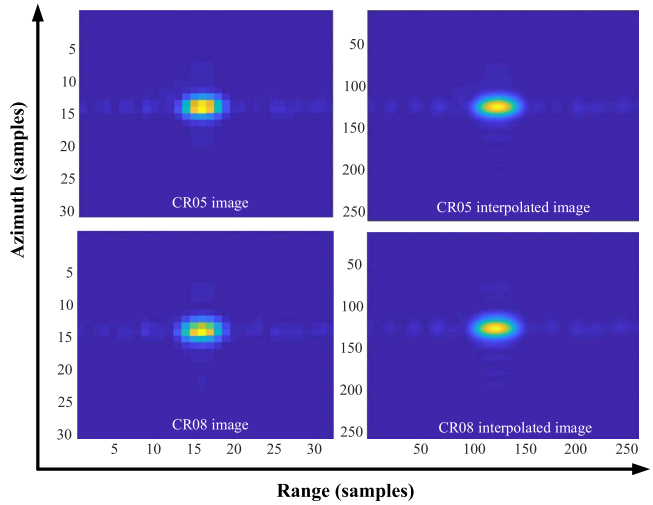

Fig. 12. Interpolated image of California CR05 and CR08.

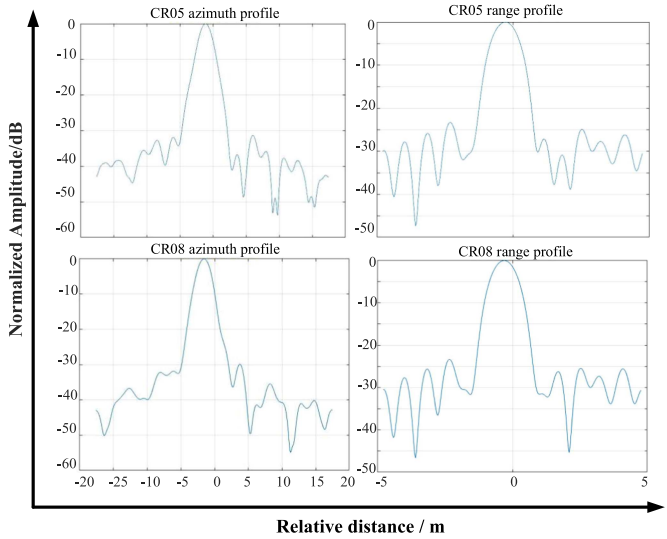

Fig. 13. Azimuth/range profile of California CR05 and CR08.

REFERENCES

[1] S. V. Baumgartner and G. Krieger, "Simultaneous high-resolution wide-swath SAR imaging and ground moving target indication: Processing approaches and system concepts," *IEEE J. Sel. Topics Appl. Earth Observ. Remote Sens.*, vol. 8, no. 11, pp. 5015–5029, Nov. 2015, doi: 10.1109/JSTARS.2015.2450019.

[2] A. Freeman and J. C. Curlander, "Radiometric correction and calibration of SAR images," *Photogrammetric Eng. Remote Sens.*, vol. 55, pp. 1295–1301, 1989.

[3] C. Wyatt, *Radiometric Calibration: Theory and Methods*. Amsterdam, The Netherlands: Elsevier, 2012.

[4] Z. Xiao et al., "Experimental study on field calibration of spaceborne SAR sensor-taking TerraSAR-X satellite as an example," *Remote Sens. Technol. Appl.*, vol. 5, 2014, Art. no. 8.

[5] Y. Zhou, L. Zhuang, J. Duan, F. Zhang, and W. Hong, "Synthetic aperture radar radiometric cross calibration based on distributed targets," *IEEE J. Sel. Topics Appl. Earth Observ. Remote Sens.*, vol. 15, pp. 9599–9612, 2022, doi: 10.1109/JSTARS.2022.3217285.

[6] S. Du, J. Hong, Y. Wang, K. Xing, T. Qiu, and J. Huang, "The influence of the azimuth RCS pattern of calibrator on SAR absolute calibration," *IEEE Geosci. Remote Sens. Lett.*, vol. 19, 2022, Art. no. 4020305, doi: 10.1109/LGRS.2021.3120433.

[7] B. J. Doering, J. Reimann, S. Raab, M. Jirousek, D. Rudolf, and M. Schwerdt, "The three-transponder method: A novel approach for traceable (E)RCS calibration of SAR transponders," in *Proc. 11th Eur. Conf. Synthetic Aperture Radar*, 2016, pp. 1–4.
[8] M. Y. Tao, P. Ji, and Y. B. Huang, "Spaceborne SAR radiometric calibration and its accuracy analysis," *Chin. Space Sci. Technol.*, vol. 35, no. 05, pp. 64–70, 2015.
[9] J. P. Peng, C. B. Ding, and H. L. Peng, "Error analysis of spaceborne SAR radiometric calibration and gain calculation of imaging processor," *J. Electron.*, vol. 35, no. 05, pp. 64–70, 2000.
[10] S. Y. Kim and N. H. Myung, "An optimal antenna pattern synthesis for active phased array SAR based on particle swarm optimization and adaptive weighting factor," *Prog. Electromagnetics Res. C*, vol. 10, no. 10, pp. 129–142, 2009.
[11] A. Freeman, "SAR calibration: An overview," *IEEE Trans Geosci. Remote Sens.*, vol. 30, no. 6, pp. 1107–1121, Nov. 1992.
[12] M. Shimada, "Radiometric and geometric calibration of JERS-1 SAR," *Adv. Space Res.*, vol. 17, no. 1, pp. 79–88, 1996, doi: 10.1016/0273-1177(95)00452-K.
[13] H. Wang et al., "Calibration of the copolarized backscattering measurements from Gaofen-3 synthetic aperture radar wave mode imagery," *IEEE J. Sel. Topics Appl. Earth Observ. Remote Sens.*, vol. 12, no. 6, pp. 1748–1762, Jun. 2019, doi: 10.1109/JSTARS.2019.2911922.
[14] Z. Manfred and B. Richard, "X-SAR radiometric calibration and data quality," *IEEE Trans Geosci. Remote Sens.*, vol. 33, no. 4, pp. 840–847, Jul. 1995.
[15] Z. Q. Wei, *Synthetic Aperture Radar Satellite*. Beijing, China: Science Press, 2001.
[16] J. C. Curlander and R. N. Mcdonough, *Synthetic Aperture Radar: Systems and Signal Processing*. Hoboken, NJ, USA: Wiley, 1991.
[17] I. G. Cumming and F. H. Wong, *Digital Processing of Synthetic Aperture Radar Data: Algorithms and Implementation*. Norwood, MA, USA: Artech House, 2005.
[18] M. Skolnik, *Radar Handbook*. New York, NY, USA: McGraw-Hill, 1990.
[19] A. Freeman, "Radiometric calibration of SAR image data," *Int. Arch. Photogramm. Remote Sens.*, vol. 29, 1993, Art. no. 212.
[20] K. Dumper, P. S. Cooper, A. F. Wons, C. J. Condley, and P. Tully, "Spaceborne synthetic aperture radar and noise jamming," in *Proc. Radar 97 (Conf. Publ. No. 449)*, Edinburgh, UK, 1997, pp. 411–414, doi: 10.1049/cp:19971707.
[21] M. Schwerdt et al., "Independent verification of the sentinel-1A system calibration," *IEEE J. Sel. Topics Appl. Earth Observ. Remote Sens.*, vol. 9, no. 3, pp. 994–1007, Mar. 2016, doi: 10.1109/JSTARS.2015.2449239.
[22] B. Brautigam, J. H. Gonzalez, M. Schwerdt, and M. Bachmann, "TerraSAR-X instrument calibration results and extension for TanDEM-X," *IEEE Trans. Geosci. Remote Sens.*, vol. 48, no. 2, pp. 702–715, Feb. 2010, doi: 10.1109/TGRS.2009.2030673.
[23] H. Wakabayashi, N. Ito, and T. Hamazaki, "PALSAR system on the ALOS," in *Proc. SPIE 3498, Sensors, Syst., Next-Gener. Satellites II*, Dec. 21, 1998, doi: 10.1117/12.333628.
[24] A. L. Gray, P. W. Vachon, C. E. Livingstone, and T. I. Lukowski, "Synthetic aperture radar calibration using reference reflectors," *IEEE Trans. Geosci. Remote Sens.*, vol. 28, no. 3, pp. 374–383, May 1990.
[25] I. M. H. Ulander, "Accuracy of using point targets for SAR calibration," *IEEE Trans. Aerosp. Electron. Syst.*, vol. 27, no. 1, pp. 139–148, Jan. 1991, doi: 10.1109/7.68156.
[26] O. Quegan et al., *Understanding Synthetic Aperture Radar Images*. Beijing, China: Electronic Industry Press, 2009.
[27] H. Jun, M. Feng, and H. Jiwei, "Current situation and development trend of inflight antenna pattern measurement techniques of spaceborne SAR," *J. Radar*, vol. 1, no. 3, pp. 217–224, 2012, doi: 10.3724/SP.J.1300.2012.20063.
[28] W. Xiaolin, "On-orbit test of spaceborne SAR antenna pattern," Ph.D. dissertation, Graduate School China Acad. Sci., Inst. Electronics, Beijing, China.
[29] M. Shimada and A. Freeman, "A technique for measurement of spaceborne SAR antenna patterns using distributed targets," *IEEE Trans. Geosci. Remote Sens.*, vol. 33, no. 1, pp. 100–114, Jan. 1995.
[30] J. Alvarez-Perez, M. Schwerdt, and M. Bachmann, "TerraSAR-X antenna pattern estimation by a complex treatment of rain forest measurements," in *Proc. IEEE Int. Symp. Geosci. Remote Sens.*, 2006, pp. 3857–3860.
[31] M. Bachmann, M. Schwerdt, and B. Brautigam, "TerraSAR-X antenna calibration and monitoring based on a precise antenna model," *IEEE Trans. Geosci. Remote Sens.*, vol. 48, no. 2, pp. 690–701, Feb. 2010.
[32] R. K. Moore and M. Hemmat, "Determination of the vertical pattern of the SIR-B antenna," *Int. J. Remote Sens.*, vol. 9, no. 5, pp. 839–847, 1988, doi: 10.1080/01431168808954899.
[33] K. Letsch and P. Berens, "Improved PSLR estimation from SAR images by consideration of the clutter background," in *Proc. 6th Eur. Conf. Synthetic Aperture Radar*, Dresden, Germany, 2006.
[34] C. Boni, M. Richard, and S. Barbarossa, "Optimal configuration and weighting of nonuniform arrays according to a maximum ISLR criterion," in *Proc. IEEE Int. Conf. Acoust.*, 1994, vol. 5, pp. V/157–V/160, doi: 10.1109/ICASSP.1994.389424.
[35] L. Dell'Amore, J.-L. Bueso-Bello, P. Klenk, J. Reimann, and P. Rizzoli, "Characterization of tropical rainforest for X-band spaceborne SAR calibration using TanDEM-X data," in *Proc. IEEE Int. Geosci. Remote Sens. Symp.*, 2023, pp. 1477–1480.

Huijuan Li received the B.S. and M.S. degrees in electronic communication engineering from the Tianjin University of Technology and Civil Aviation University of China, Tianjin, China, in 2018 and in 2021, respectively.

She is currently with China SiWei Surveying and Mapping Technology Company, Ltd., Beijing, China. Her research interests include spaceborne synthetic aperture radar (SAR) imaging and radiometric calibration.

Heng Zhang (Member, IEEE) received the M.S. degree in signal processing from the University of Chinese Academy of Sciences, Beijing, China, in 2016.

He is currently with China SiWei Surveying and Mapping Technology Company, Ltd., Beijing, China. He was a senior engineer in this field. His main research interests include advanced spaceborne synthetic aperture radar (SAR) techniques and data processing, including geometric calibration of SAR.

Qi Chen received the Ph.D. degree in communication and information systems from the Graduate School of Chinese Academy of Sciences, Beijing, China, in 2007.

In July 2016, he was a research fellow China Aerospace Science and Technology Corporation. He is currently with China SiWei Surveying and Mapping Technology Company, Ltd., Beijing, China. His research interests include spaceborne synthetic aperture radar imaging and modern signal processing.

Yongpeng Gao (Member, IEEE) received the B.S and M.S. degrees in engineering of information and conmmunication from the Beijing Institute of Technology, Beijing, China, in 2019 and 2022, respectively.

He is currently with the China SiWei Surveying and Mapping Technology Company, Ltd., Beijing, China. His research interests include spaceborne synthetic aperture radar imaging and moving target radar imaging.

Xiaoyu Shi received the B.S. and M.S. degrees in geodesy and survey engineering from the Nanjing Tech University and China University of Mining and Technology, Beijing, China, in 2018 and in 2021, respectively.

She is currently with China SiWei Surveying and Mapping Technology Company, Ltd., Beijing, China. Her research interests include geometric calibration of spaceborne synthetic aperture radar and atmospheric delay correction.

Lifeng Zhang received the B.S. and M.S. degrees in surveying and mapping engineering from the Xinjiang University, Xinjiang, China, and Liaoning Technical University, Fuxin, China, in 2018 and in 2021, respectively.

He is currently with China SiWei Surveying and Mapping Technology Company, Ltd., Beijing, China. His research interests include geometric correction and baseline calibration of spaceborne synthetic aperture radar.